

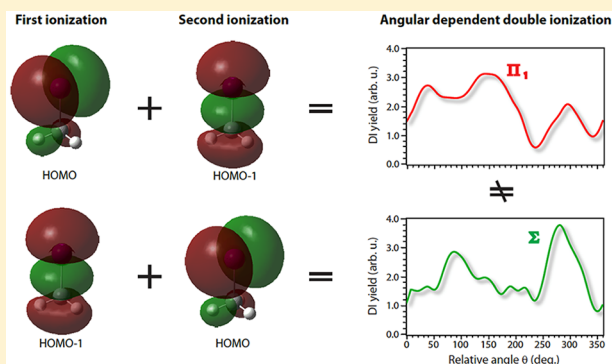
Disentangling Strong-Field Multielectron Dynamics with Angular Streaking

Alexander H. Winney, Gihan Basnayake,¹ Duke A. Debrah,¹ Yun Fei Lin, Suk Kyoung Lee, Paul Hoerner, Qing Liao, H. Bernhard Schlegel,¹ and Wen Li*¹

Department of Chemistry, Wayne State University, Detroit, Michigan 48202, United States

Supporting Information

ABSTRACT: The study into the interaction between a strong laser field and atoms/molecules has led to significant advances in developing spectroscopic tools in the attosecond time-domain and methods for controlling chemical reactions. There has been great interest in understanding the complex electronic and nuclear dynamics of molecules in strong laser fields. However, it is still a formidable challenge to fully model such dynamics. Conventional experimental tools such as photoelectron spectroscopy encounter difficulties in revealing the involved states because the electron spectra are largely dictated by the property of the laser field. Here, with strong field angular streaking technique, we measure the angle-dependent ionization yields that directly reflect the symmetry of the ionizing orbitals of methyl iodide and thus reveal the ionization/dissociation dynamics. Moreover, kinematically complete measurements of momentum vectors of all fragments in dissociative double ionization processes allow access to electron-momentum correlations that reveal correlated multielectron dynamics.



The response of atoms and molecules to a strong laser field ($>10^{13}$ W/cm², corresponding to a laser peak E-field ~ 0.02 a.u. or 10^8 V/cm) is an interesting and significant topic, which has been subjected to intense investigation in the past three decades. Two aspects of strong field dynamics are particularly appealing. First, the strong field interaction with atoms can lead to the production of attosecond pulses through a nonlinear process called high-harmonic generation,^{1,2} in which electrons are repeatedly driven away and pulled back toward the ionic core by the oscillating laser electric field, and this oscillating dipole emits bursts of attosecond light pulses in the extreme ultraviolet and soft-X-ray spectra range. Attosecond pulses are highly desirable in implementing time-resolved studies operating in the attosecond time-scale.³ Strong field processes themselves can also probe attosecond dynamics by exploiting the *chirped re-encounter* (the returning electrons arrive at the ion core at different time with different energies so that the energy-time correlation can be exploited to achieve subfemtosecond time resolution) between the ions and the electrons that are ionized approximately half a laser period (1.3 fs for a typical 800 nm laser) earlier. This has been demonstrated in both high harmonic spectroscopy^{4,5} and high-order above-threshold ionization.⁶ The second aspect of strong field interaction is in the capability of strong field control of chemistry. The significant distortion of the potential energy landscape generated by strong fields provides a tantalizing prospect of *potential surface engineering* for guiding chemical reactions. This concept was explored in many coherent control

experiments,^{7–9} and recently we have shown in theory that strong mid-IR pulses can achieve the long-standing goal of mode-selective chemistry.^{10,11} Among all these current and future applications of strong field dynamics, the topic of unraveling the complex strong field ionization dynamics, i.e., the initiation step of strong field phenomena, remain a central component but is still challenging.

The interactions of intense laser pulses with atoms have been described by a single active electron and quasi-static pictures, suggesting prevailing ionization from the highest electronic orbitals.

The interactions of intense laser pulses with atoms have been described by a single active electron and quasi-static pictures, suggesting prevailing ionization from the highest electronic orbitals. However, many studies in polyatomic systems have shown that multielectron effects should be considered for better understanding of strong field ionization.^{5,12–14} One

Received: January 4, 2018

Accepted: April 27, 2018

Published: April 27, 2018

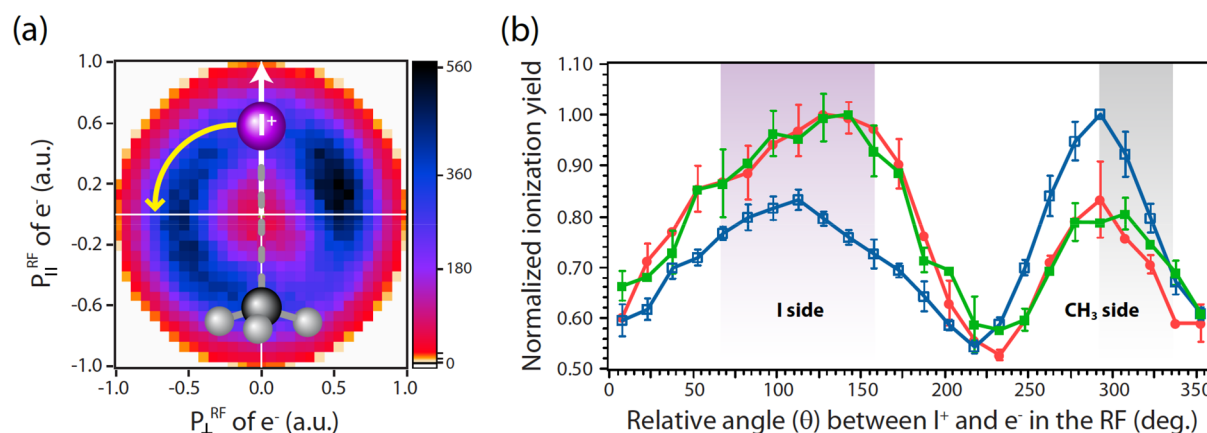


Figure 1. (a) Recoil-frame electron momentum distribution obtained by coincidence measurements of electrons and I^+ for the dissociative single ionization of CH_3I . The I^+ recoil momentum is pointed up, indicated by the white arrow and the yellow curved arrow shows the helicity of the circularly polarized light. (b) RFPADs for dissociative single ionization (blue line with open square points) and dissociative double ionization measured with quadruple coincidence (green line with closed square points, $e_1 + e_2 + \text{fragment1} + \text{fragment2}$) and double coincidence (red line with closed circle points, $e + \text{fragment}$), respectively. The angle θ is defined as the relative angle between the recoil direction of the iodine ion and the ejected electron (the angle increases anticlockwise). The gray and purple shaded areas correspond to the distributions of electrons escaping from the CH_3 and I sides, respectively. Note that the two curves were normalized to their own maxima.

powerful method for interrogating this effect on the strong field ionization dynamics is to determine the molecular frame photoelectron angular distribution (MFPAD), which can reflect the structure of ionizing orbitals. The measurement of MFPAD employing the principle of angular streaking^{15,16} has been demonstrated for randomly oriented diatomics¹⁴ and laser-oriented molecules.¹⁷ A more refined technique was demonstrated by combining the channel-resolved above threshold ionization (CRATI) method,^{18,19} in which above-threshold ionization (ATI) combs are measured to identify the channel of interest, with laser alignment to obtain the channel- and angle-resolved ionization yields in the molecular frame.²⁰ However, at moderately high laser intensities ($\sim 1 \times 10^{14}$ W/cm²) or for extremely short few-cycle pulses, ATI peaks would become less evident due to significant Stark shifts,^{21–23} potential non-adiabatic electron dynamics,^{24,25} and carrier-envelope phase dependence.²⁶

Furthermore, a direct measurement of MFPAD for double ionization of polyatomics is highly desirable for investigating correlated multielectron dynamics. Such measurements have encountered technical difficulties that limit the coincidence detection of two electrons. Here in this work, we show that the angular streaking technique coupled with electron–ion coincidence can be applied to polyatomic systems to measure the recoil-frame photoelectron angular distributions (RFPAD) of single and double ionization. With the help of theoretical modeling, the dynamics of these processes can now be understood in unprecedented detail. We also show the first 2D photoionization map that reveals correlated angular-dependent double ionization probabilities. We demonstrated these new capabilities in methyl iodide, a polyatomic molecule that has been subjected to intensive investigation. For example, the asymmetric emission measured from two-color femto-second experiments on CH_3I by Walt et al. suggested that dissociative single ionization occurs mostly from the HOMO via a possible bond-softening due to a strong coupling with an excited dissociative state or from vibrationally excited cations by recollision,²⁷ while Luo et al.²⁸ proposed that ionization from HOMO–1 is the leading contribution to fragmentation, based on measuring the alignment-dependent evolution of ion yield.

An orientation-resolved PAD can offer a definitive answer but has not been achieved. Furthermore, it was not clear whether lower lying orbitals such as HOMO–2 play a major role in dissociative double ionization of methyl iodide even though a plethora of experimental methods have been applied to study this system.^{27–31} It is worth noting that all previous investigations employed linearly polarized light, with which electron recollision dynamics could play an important role to induce multiple ionization.

Recently, we introduced the 3D two-electron angular streaking (3D-2eAS) technique, which can probe electron dynamics within 1 fs between two electrons produced in strong field double ionization.³² In this study, we have upgraded the 3D-2eAS coincidence apparatus (see Figure 1 in ref 32 for a detailed depiction) by adding an additional camera for ions in order to detect full 3D momenta of both ions and coincident electrons. In the following, we will briefly describe the experimental setup. Circularly polarized 800 nm light with a pulse width of 30 fs was focused onto the molecular beam using a spherical mirror in the vacuum. The estimated laser intensity and ellipticity were $\sim 1 \times 10^{14}$ W/cm² and ~ 0.9 . The methyl iodide beam was generated by bubbling helium carrier gas through a liquid methyl iodide sample and into the source chamber. The beam was double-skimmed before entering the main chamber, in which it was intercepted by the laser beam and ionized. The produced electrons and ions were accelerated with an inhomogeneous electric field toward the opposite ends of the time-of-flight tube, where they impacted two MCP/phosphor screen detectors. The positions of both electrons and ions were registered by two cameras, which have a resolution of 448×448 pixels (with the detector diameter of 75 mm, the system has a native spatial resolution ~ 160 μm) at a frame rate of 1 kHz. With a high-speed digitizer, the TOF of each particle was also registered to provide complete 3D momenta of ions and electrons in coincidence.^{33,34} Then the PAD was plotted with respect to a fixed ion momentum direction in the plane of the polarization to produce the RFPAD. The false coincidence rate was estimated to be $\sim 16\%$. The capability to directly detect both electrons in coincidence with dissociative double

ionization enables us to study electron correlation in double ionization.

At the laser intensity used in this study, a parent cation (CH_3I^+) was the main product, but we also observed significant amounts of I^+ ($\sim 6\%$ of the parent cation yield) and CH_3^+ ($\sim 2\%$ of the parent cation) fragment ions resulting from dissociative single ionization. Dissociative and nondissociative double ionizations were about 2% and 0.2% of the parent cation yield, respectively. For single ionization, the kinetic energy release (KER) of I^+ was peaked at 0.07 eV (which corresponds to a total KER of 0.7 eV) while the KER of CH_3^+ was peaked close to zero eV. Both results are consistent with many previous measurements.^{29,30} In our study, by detecting the recoil momentum of I^+ and CH_3^+ and the coincidence electrons in the dissociative single ionization process, we obtained the recoil-frame photoelectron angular distribution (RFPAD) shown in Figure 1a. While the ion momentum distribution is isotropic in the plane of polarization due to the rotating electric field of the circularly polarized light, the observed strong anisotropy of ion momentum in the plane perpendicular to the polarization plane of the circularly polarized light (data not shown) suggests that a fast dissociation with respect to rotation is at play and thus validates the axial recoil approximation. The strong anisotropic angular distribution of fragments was also observed for the dissociative double ionization process (data not shown), which is not surprising considering the multiple charges. According to the angular streaking principle, the final momentum of electrons released along the C–I bond will be rotated about 90 deg away from the recoil direction of the ion because the vector potential of the instantaneous electric field at the moment of ionization is orthogonal to the direction of the electric field. The vector potential primarily determines the final momentum of the electrons in the laser field. It is worth noting that there are no clear ATI peaks observed in our experiment. With the known helicity of the circularly polarized light, we can further identify from which site (I or CH_3) the electrons are ionized. This is a major advantage of employing the angular streaking technique. In methyl iodide, it was found that the electrons are ejected from the I and CH_3 sides, corresponding to the black broad and narrow features (islands) in the left and right side of Figure 1a, respectively. The slight deviation from 90° to the I^+ recoil direction is due to the attractive interaction between the departed electron and the remaining ionic core. Figure 1b shows the angular-dependent ionization yield (blue line with open squares) obtained by radially integrating the electron momentum distribution seen in Figure 1a. We also obtained the RFPAD for the channel that leads to CH_3^+ by plotting the PAD with respect to the momentum of CH_3^+ recoil. The results (not shown) are similar to the channel leading to I^+ dissociation.

The distinctive RFPAD is clearly a representation of angular-dependent ionization yields of different contributing orbitals. We theoretically examined the different angular-dependent ionization yields for single and double ionization by the time-dependent configuration interaction with a complex absorbing potential (TDCI-CAP) method.^{35–37} Calculations were performed by using the aug-cc-pVTZ basis set, associated pseudopotentials for iodine,³⁸ and an additional 15 sets of diffuse functions on each atom. Static electric fields along different directions were employed in the calculation to map the angular-dependent ionization yields. The detailed methodology for calculating the angular dependence of ionization of the methyl halides was thoroughly tested (see detailed method

description in the Supporting Information).³⁷ The degenerate highest occupied molecular orbitals (HOMOs), the first lower-lying orbital (HOMO–1), and their calculated angular-dependent ionization yields are displayed in Figure 2a,b. The

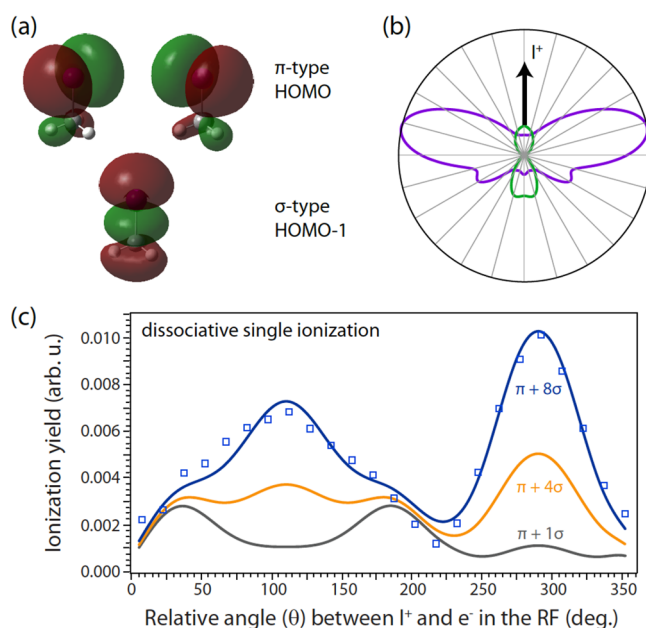


Figure 2. (a) Electron density plots of the degenerate highest occupied molecular orbitals (HOMO) and HOMO–1 of CH_3I . (b) Contributions to the calculated angular-dependent ionization yields from different orbitals: π -type HOMO (purple), and σ -type HOMO–1 (green) for static electric fields of 0.055 au (1.06×10^{14} W/cm²). The C–I bond orientation is indicated by the I^+ recoil direction. (c) Comparison between experimental and calculated angular-dependent ionization yield, with which different weighting factors between HOMO and HOMO–1 ionization are used. The calculated results include a 10-degree convolution, accounting for angle uncertainty due to deviation from the axial recoil approximation. Comparison with experiment indicates that the contribution from the σ orbital (yielding the A state of CH_3I^+) needs to be increased by a factor of 8 to account for the greater efficiency of generating fragment ions from A state of CH_3I^+ than from the X state.

HOMO is a doubly degenerate pair of π -type orbitals from the lone pairs on the I atom, contributing to a broader ionization probability with peaks nearly perpendicular (75°) to the recoil axis. On the other hand, the HOMO–1 is a σ -type orbital that is responsible for C–I bonding, contributing to the dominant ionization probability along the molecular axis. HOMO–2 (not shown here) has a maximal electron density on the CH_3 side, suggesting that ionization of this orbital is predominantly from the CH_3 side.

For single ionization, even though our calculation shows that the ionization yields contributed from the HOMO is the largest, the angular dependence accounting for the HOMO alone cannot explain our experimental result: a significant CH_3 site ionization was identified, as shown in Figure 1. This is, however, not surprising because we are measuring a dissociative ionization channel. Removing an electron from HOMO produces the electronic ground state of parent cations (X^2E) that is known to be strongly bound.^{30,39} Direct HOMO–1 (σ -type orbital) ionization turns out to be the dominant channel that leads to I^+ production: first, our theoretical modeling suggests HOMO–1 orbital has higher contribution to

ionization probability on the CH₃ side than on the I side as indicated in Figure 2b; second, by enhancing the contribution from HOMO-1 to account for the greater yield of fragment ions from the A state of CH₃I⁺, the experimental angular-dependent ionization yield is nicely reproduced (Figure 2c). This indicates that 72% of the ion yield comes from the A state of CH₃I⁺ and 28% from the X state. It is still surprising to see a nonzero contribution from the X state considering its high bond dissociation energy (BDE) (~3 eV). This can take place from the X state by further absorption of two photons to the A²A₁ state or if the produced X state is highly vibrationally excited with an internal energy above its BDE. The former process has been well documented using resonance two-photon dissociation spectroscopy⁴⁰ and is likely at play here. While the A state is also stable with a smaller BDE (~4 eV), vibrationally excited A states can dissociate readily. It is worth noting that the A state is adiabatically connected to the CH₃⁺+I asymptote and nonadiabatically connected to the I⁺+CH₃ asymptote.⁴¹ The similarly looking RFPADs of these two channels suggest that the initial ionization shares a common process with both X and A state cations contribution, while the coupled nuclear and electronic dynamics away from the Franck–Condon regions determine the final products. The dissociation process involves both charge transfer and nonadiabatic transitions and is an excellent system for future time-resolved studies.

The dissociation process involves both charge transfer and non-adiabatic transitions and is an excellent system for future time-resolved studies.

The angular dependence of ionization for the dissociative double ionization (green line with closed squares in Figure 1b) was obtained by detecting two electrons and two fragment ions (a quadruple coincidence). This is in good agreement with the results obtained by measuring double coincidence events between one electron and one iodine ion with a selected total kinetic energy (~4.5 eV) corresponding to double ionization (red line with closed circles). This validates our quadruple coincidence measurements, from which we can study correlated electron dynamics. A clear difference is seen between dissociative single and double ionization: electrons produced from the dissociative double ionization are primarily from the I side, suggesting important contributions from the Π orbital (see Figure 2a).

Because circularly polarized light was used, recollision is suppressed in methyl iodide, and thus only sequential double ionization needs to be considered.⁴² We consider the lowest-energy pathways for producing dications: HOMO(Π), HOMO(\perp), and HOMO-1 orbital ionization in neutrals followed by a second ionization of corresponding cations, which we call Π_1 , Π_2 , and Σ cations, respectively. HOMO(Π) and HOMO(\perp) are the two degenerate orbitals lying parallel and perpendicular to the plane of the polarization of the circularly polarized light. Theoretically, we first extracted the orbital-resolved angular-dependent ionization yields similar as in treating neutral ionization; then we calculated the angular-dependent yields of the ionization of Π_1 , Π_2 , and Σ cations (Figure 3a). We produced three angular-dependent ionization yields for three different ionization processes: (1) HOMO(Π)

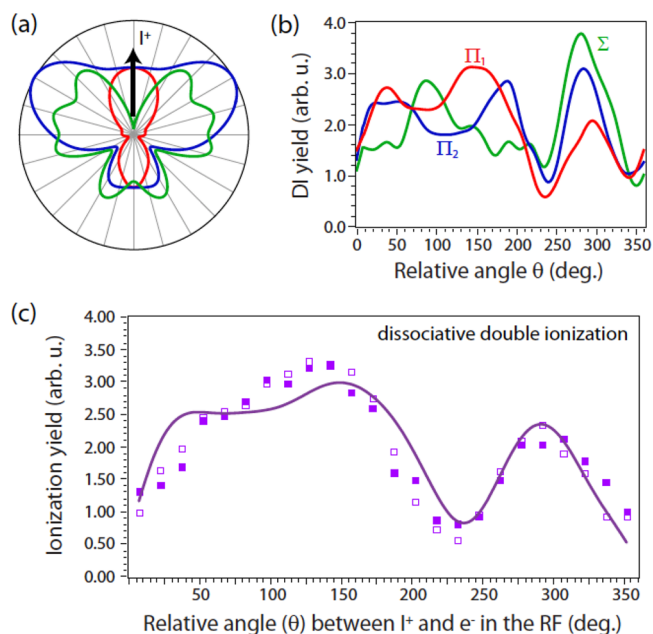


Figure 3. (a) Calculated angular-dependent ionization yields for Π_1 (red), Π_2 (blue), and Σ (green) cations at a field strength of 0.065 au (1.48×10^{14} W/cm²). (b) The angular-dependent double ionization yield for three different pathways with Π_1 (red), Π_2 (blue) and Σ (green) cations as the intermediate states. The displayed asymmetry of each curve reflects a 10-degree angle shift between the first and second ionization due to the different Coulomb interactions between the ionic core and the departing electron. (c) Comparison between experimental (solid square from quadruple coincidence measurement, empty square from double coincidence measurement) and calculated angular-dependent ionization yield (purple line) for dissociative double ionization. The calculated result used a weighting factor of 0.68:0.2:0.11 for Π_1 , Σ and Π_2 cation pathways, respectively. The calculated result also included a 10-degree convolution accounting for angular uncertainty due to deviation from the axial recoil approximation. Both the x-axes in panels b and c show the relative angle between I⁺ and electron momentum vectors.

→ Π_1 cation → dication ($\sigma^1\pi_1^1\pi_2^2$), (2) HOMO(\perp) → Π_2 cation → dication ($\sigma^2\pi_1^1\pi_2^1$) and (3) HOMO-1 → Σ cation → dication ($\sigma^1\pi_1^1\pi_2^2$). We achieved this by normalizing the curve of each single ionization step to 1 and then summed the two curves. To fit the final experimental data, which showed a clear asymmetry for the feature at 120 degrees, a 10-degree angle shift was added between the first and second ionization to account for the different Coulomb interactions between the ionic core (singly and doubly charged) and the departing electron. The results are shown in Figure 3b. It is interesting to point out even though the electron configurations of the final dications for the first and third processes are the same: both losing one electron from the HOMO and one from the HOMO-1, the angular-dependent ionization is significantly different (the red and green lines in Figure 3b). This suggests that the order of losing electrons is important and the orbital reorganization and relaxation taking place between the first and second ionization is significant. Figure 3c shows that the experimental result is reasonably reproduced by the weighted sum of the three channels with a ratio of 0.68:0.20:0.11. The overall agreement validates the employed theoretical method for modeling strong field double ionization. The branching ratios are from the calculations directly, which suggests the majority of the dications are dissociative. A discrepancy

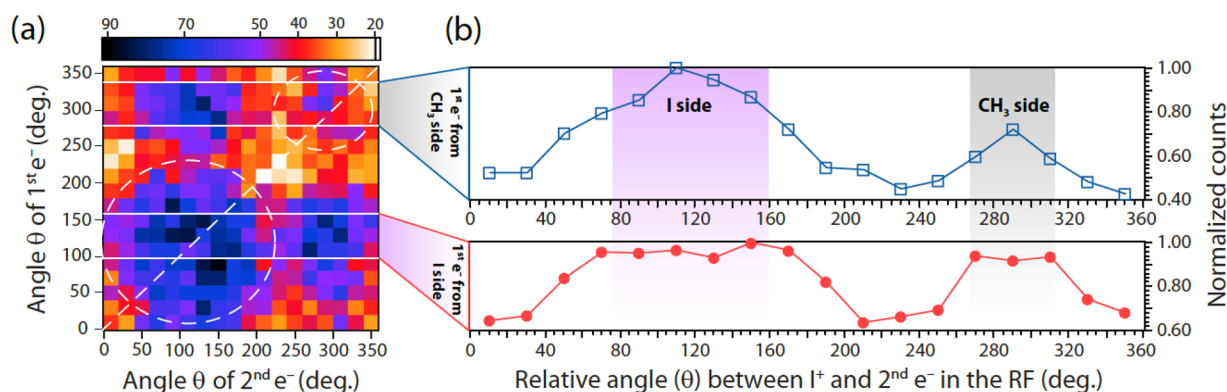


Figure 4. (a) 2D electron–electron angular correlation in the recoil frame of the dissociative double ionization of CH_3I . The angle θ is defined as the relative angle between the recoil direction of the iodine ion ($\theta = 0^\circ$) and the ejected electron. The white dashed ovals indicate the two diagonal peaks. (b) Angular-dependent ionization yields of the second electron in the recoil frame. The top panel corresponds to the case when the first electron is released from the I side, and the bottom panel corresponds to the case when the first electron is released from the peak in the CH_3 side (compare with Figure 1b).

between experiments and theory on the width of the peak around 120 degrees is likely due to the fact that the current calculations did not include pulse intensity average but used a single field strength of 0.045 a.u. for neutral ionization and 0.065 a.u. for cation ionization.

The multielectron dynamics involved in the dissociative double ionization can be understood in more detail by investigating the correlated double ionization dynamics.

The multielectron dynamics involved in the dissociative double ionization can be understood in more detail by investigating the correlated double ionization dynamics. Here, the angular-dependent ionization yields of the first and second electron are plotted in a 2D graph, shown in Figure 4a. As far as we know, this is the first presentation of such data, and we call it a 2D photoionization spectrum. As demonstrated previously,^{32,43} this can now be achieved because of the high electron–electron coincidence capability of our apparatus. In this plot, the diagonal peaks represent the case of both electrons being ionized from the same site of the molecule while off-diagonal peaks are for sequential ionizations from two different sites. In Figure 4a, we see two peaks of each kind showing that both cases are present in methyl iodide. However, the intensities of the peaks are quite different. The diagonal peak at $(290^\circ, 290^\circ)$ is significantly weaker than the other peaks, which suggests that sequential ionizations from only CH_3 site is not favored. Considering that CH_3 site ionization is mainly from low-lying orbitals such as HOMO–1 and HOMO–2, this can be explained by the fact that ionization from two low-lying orbitals will produce highly excited dications, which have lower ionization probability. On the other hand, the strongest diagonal feature at $(120^\circ, 120^\circ)$ shows that it is highly favored that both electrons are ionized from the I site. From our calculation, we understand such a preference does not arise from ionization of two electrons from the same HOMO orbital. Instead this is due to the dominant double ionization channel $\text{HOMO}(\text{II}) \rightarrow \Pi_1$ cation \rightarrow dication,

in which each ionization step is dominated by ionizing electron from the I side.

In summary, we measured the RFPAD for the dissociative single and double ionization of methyl iodide using a newly developed 3D two-electron angular streaking (3D-2eAS) technique. Fragmentation of CH_3I is initiated via ionization from multiple orbitals, whose relative contributions have been determined with the help of TDCI-CAP calculations. The full 3D momentum measurement of two electrons in double ionization enables us to study correlated ionization dynamics. This technique provides an efficient and direct way to study the complex multiorbital and multielectron effects on strong field ionization. The correlated double ionization can be viewed from another perspective shown in Figure 4b, in which we plot the angular-dependent ionization yields of the second electron with the first electron being ionized from either the CH_3 or I side. We can see the second ionization from the CH_3 side is enhanced if the first ionization is from the I side. Note that the designation of the first and second electron is arbitrary in this case. This finding has the same origin as the weak diagonal peak at $(290^\circ, 290^\circ)$. However, this new perspective provides a new method for studying electron-correlation driven nonadiabatic dynamics in the attosecond time domain, in which two electron's dynamics are correlated even at the subcycle level.^{24,44} With the angular streaking method, the relative ejection angle between the electrons can be mapped into a time delay with a resolution of tens of attoseconds. By using few-cycle pulses, which enables differentiation of the first and the second ionization by the magnitude of the electron momentum,¹⁵ and restricting electron dynamics within one or half a laser cycle, it is possible now to directly capture such dynamics.

■ ASSOCIATED CONTENT

Supporting Information

The Supporting Information is available free of charge on the ACS Publications website at DOI: 10.1021/acs.jpcllett.8b00028.

Theoretical details (PDF)

■ AUTHOR INFORMATION

ORCID

Gihan Basnayake: 0000-0002-5404-5621

Duke A. Debrah: 0000-0002-1281-3012

H. Bernhard Schlegel: 0000-0001-7114-2821

Wen Li: 0000-0002-3721-4008

Notes

The authors declare no competing financial interest.

ACKNOWLEDGMENTS

This research was supported by the U.S. Department of Energy (DOE), Office of Science, Basic Energy Sciences (BES), under Award # DE-SC0012628 (CH₃I strong field dynamics), and by the U.S. Army Research Office, under Award # W911NF-12-1-0598 (the new 3D electron-ion imaging system that enables full 3D momentum measurements of both electrons and ions).

REFERENCES

- (1) Kulander, K. C.; Schafer, K. J.; Krause, J. L. Dynamics of Short-Pulse Excitation, Ionization and Harmonic Conversion. In *Super-Intense Laser-Atom Physics*; Piraux, B., L'Huillier, A., Rzazewski, K., Eds.; Plenum Press: New York, 1993; Vol. 316, pp 95–110.
- (2) Corkum, P. B. Plasma Perspective on Strong-Field Multiphoton Ionization. *Phys. Rev. Lett.* **1993**, *71*, 1994–1997.
- (3) Feist, J.; Nagele, S.; Pazourek, R.; Persson, E.; Schneider, B. I.; Collins, L. A.; Burgdorfer, J. Probing Electron Correlation Via Attosecond XUV Pulses in the Two Photon Double Ionization of Helium. *Phys. Rev. Lett.* **2009**, *103*, 063002.
- (4) Baker, S.; Robinson, J. S.; Haworth, C. A.; Teng, H.; Smith, R. A.; Chirila, C. C.; Lein, M.; Tisch, J. W. G.; Marangos, J. P. Probing Proton Dynamics in Molecules on an Attosecond Time Scale. *Science* **2006**, *312*, 424–427.
- (5) Smirnova, O.; Mairesse, Y.; Patchkovskii, S.; Dudovich, N.; Villeneuve, D.; Corkum, P.; Ivanov, M. Y. High Harmonic Interferometry of Multi-Electron Dynamics in Molecules. *Nature* **2009**, *460*, 972–977.
- (6) Blaga, C. I.; Xu, J.; DiChiara, A. D.; Sistrunk, E.; Zhang, K.; Agostini, P.; Miller, T. A.; DiMauro, L. F.; Lin, C. D. Imaging Ultrafast Molecular Dynamics with Laser-Induced Electron Diffraction. *Nature* **2012**, *483*, 194–197.
- (7) Brumer, P.; Shapiro, M. Coherence Chemistry: Controlling Chemical Reactions with Lasers. *Acc. Chem. Res.* **1989**, *22*, 407–413.
- (8) Assion, A.; Baumert, T.; Bergt, M.; Brixner, T.; Kiefer, B.; Seyfried, V.; Strehle, M.; Gerber, G. Control of Chemical Reactions by Feedback-Optimized Phase-Shaped Femtosecond Laser Pulses. *Science* **1998**, *282*, 919–922.
- (9) Levis, R. J.; Menkir, G. M.; Rabitz, H. Selective Bond Dissociation and Rearrangement with Optimally Tailored, Strong-Field Laser Pulses. *Science* **2001**, *292*, 709–713.
- (10) Lee, S. K.; Suits, A. G.; Schlegel, H. B.; Li, W. A Reaction Accelerator: Mid-Infrared Strong Field Dissociation Yields Mode-Selective Chemistry. *J. Phys. Chem. Lett.* **2012**, *3*, 2541–2547.
- (11) Lee, S. K.; Schlegel, H. B.; Li, W. Bond-Selective Dissociation of Polyatomic Cations in Mid-Infrared Strong Fields. *J. Phys. Chem. A* **2013**, *117*, 11202–11209.
- (12) Li, W.; Zhou, X.; Lock, R.; Patchkovskii, S.; Stolow, A.; Kapteyn, H. C.; Murnane, M. M. Time-Resolved Dynamics in N₂O₄ Probed Using High Harmonic Generation. *Science* **2008**, *322*, 1207.
- (13) McFarland, B. K.; Farrell, J. P.; Bucksbaum, P. H.; Gühr, M. High Harmonic Generation from Multiple Orbitals in N₂. *Science* **2008**, *322*, 1232.
- (14) Akagi, H.; Otobe, T.; Staudte, A.; Shiner, A.; Turner, F.; Dörner, R.; Villeneuve, D. M.; Corkum, P. B. Laser Tunnel Ionization from Multiple Orbitals in HCl. *Science* **2009**, *325*, 1364–1367.
- (15) Ecker, P.; Smolarski, M.; Schlup, P.; Biegert, J.; Staudte, A.; Schöffler, M.; Müller, H. G.; Dörner, R.; Keller, U. Attosecond Angular Streaking. *Nat. Phys.* **2008**, *4*, 565–570.
- (16) Pfeiffer, A. N.; Cirelli, C.; Smolarski, M.; Dörner, R.; Keller, U. Timing the Release in Sequential Double Ionization. *Nat. Phys.* **2011**, *7*, 428–433.

(17) Holmegaard, L.; Hansen, J. L.; Kalhoj, L.; Louise Kragh, S.; Stapelfeldt, H.; Filsinger, F.; Kupper, J.; Meijer, G.; Dimitrovski, D.; Abu-samha, M.; Martiny, C. P. J.; Bojer Madsen, L. Photoelectron Angular Distributions from Strong-Field Ionization of Oriented Molecules. *Nat. Phys.* **2010**, *6*, 428–432.

(18) Boguslavskiy, A. E.; Mikosch, J.; Gijsbertsen, A.; Spanner, M.; Patchkovskii, S.; Gador, N.; Vrakking, M. J. J.; Stolow, A. The Multielectron Ionization Dynamics Underlying Attosecond Strong-Field Spectroscopies. *Science* **2012**, *335*, 1336–1340.

(19) Sándor, P.; Zhao, A.; Rozgonyi, T.; Weinacht, T. Strong Field Molecular Ionization to Multiple Ionic States: Direct Versus Indirect Pathways. *J. Phys. B: At., Mol. Opt. Phys.* **2014**, *47*, 124021.

(20) Mikosch, J.; Boguslavskiy, A. E.; Wilkinson, I.; Spanner, M.; Patchkovskii, S.; Stolow, A. Channel- and Angle-Resolved above Threshold Ionization in the Molecular Frame. *Phys. Rev. Lett.* **2013**, *110*, 023004.

(21) Dimitrovski, D.; Martiny, C. P. J.; Madsen, L. B. Strong-Field Ionization of Polar Molecules: Stark-Shift-Corrected Strong-Field Approximation. *Phys. Rev. A: At., Mol., Opt. Phys.* **2010**, *82*, 053404.

(22) Sussman, B. J.; Townsend, D.; Ivanov, M. Y.; Stolow, A. Dynamic Stark Control of Photochemical Processes. *Science* **2006**, *314*, 278–281.

(23) Dietrich, P.; Corkum, P. B. Ionization and Dissociation of Diatomic Molecules in Intense Infrared Laser Fields. *J. Chem. Phys.* **1992**, *97*, 3187–3198.

(24) Lezius, M.; Blanchet, V.; Rayner, D. M.; Villeneuve, D. M.; Stolow, A.; Ivanov, M. Y. Nonadiabatic Multielectron Dynamics in Strong Field Molecular Ionization. *Phys. Rev. Lett.* **2001**, *86*, 51–54.

(25) Miller, M. R.; Xia, Y.; Becker, A.; Jaroń-Becker, A. Laser-Driven Nonadiabatic Electron Dynamics in Molecules. *Optica* **2016**, *3*, 259–269.

(26) Gazibegović-Busuladžić, A.; Hasović, E.; Busuladžić, M.; Milošević, D. B.; Kelkensberg, F.; Siu, W. K.; Vrakking, M. J. J.; Lépine, F.; Sansone, G.; Nisoli, M.; Znakovskaya, I.; Kling, M. F. Above-Threshold Ionization of Diatomic Molecules by Few-Cycle Laser Pulses. *Phys. Rev. A: At., Mol., Opt. Phys.* **2011**, *84*, 043426.

(27) Walt, S. G.; Bhargava Ram, N.; von Conta, A.; Tolstikhin, O. I.; Madsen, L. B.; Jensen, F.; Wörner, H. J. Role of Multi-Electron Effects in the Asymmetry of Strong-Field Ionization and Fragmentation of Polar Molecules: The Methyl Halide Series. *J. Phys. Chem. A* **2015**, *119*, 11772–11782.

(28) Luo, S.; Hu, W.; Yu, J.; Li, X.; He, L.; Wang, C.; Liu, F.; Ding, D. Multielectron Effects in the Strong Field Sequential Ionization of Aligned CH₃I Molecules. *J. Phys. Chem. A* **2017**, *121*, 6547–6553.

(29) Liu, H.; Yang, Z.; Gao, Z.; Tang, Z. Ionization and Dissociation of CH₃I in Intense Laser Field. *J. Chem. Phys.* **2007**, *126*, 044316.

(30) Wang, Y.; Zhang, S.; Wei, Z.; Zhang, B. Velocity Map Imaging of Dissociative Ionization and Coulomb Explosion of CH₃I Induced by a Femtosecond Laser. *J. Phys. Chem. A* **2008**, *112*, 3846–3851.

(31) Corrales, M. E.; Gitzinger, G.; González-Vázquez, J.; Loriot, V.; de Nalda, R.; Bañares, L. Velocity Map Imaging and Theoretical Study of the Coulomb Explosion of CH₃I under Intense Femtosecond Ir Pulses. *J. Phys. Chem. A* **2012**, *116*, 2669–2677.

(32) Winney, A. H.; Lee, S. K.; Lin, Y. F.; Liao, Q.; Adhikari, P.; Basnayake, G.; Schlegel, H. B.; Li, W. Attosecond Electron Correlation Dynamics in Double Ionization of Benzene Probed with Two-Electron Angular Streaking. *Phys. Rev. Lett.* **2017**, *119*, 123201.

(33) Lee, S. K.; Lin, Y. F.; Lingenfelter, S.; Fan, L.; Winney, A. H.; Li, W. Communication: Time- and Space-Sliced Velocity Map Electron Imaging. *J. Chem. Phys.* **2014**, *141*, 221101.

(34) Lin, Y. F.; Lee, S. K.; Adhikari, P.; Herath, T.; Lingenfelter, S.; Winney, A. H.; Li, W. Note: An Improved 3D Imaging System for Electron-Electron Coincidence Measurements. *Rev. Sci. Instrum.* **2015**, *86*, 096110.

(35) Krause, P.; Sonk, J. A.; Schlegel, H. B. Strong Field Ionization Rates Simulated with Time-Dependent Configuration Interaction and an Absorbing Potential. *J. Chem. Phys.* **2014**, *140*, 174113.

(36) Krause, P.; Schlegel, H. B. Angle-Dependent Ionization of Hydrides Ahn Calculated by Time-Dependent Configuration Inter-

action with an Absorbing Potential. *J. Phys. Chem. A* **2015**, *119*, 10212–10220.

(37) Hoerner, P.; Schlegel, H. B. Angular Dependence of Strong Field Ionization of CH_3X ($\text{X} = \text{F}, \text{Cl}, \text{Br}, \text{or I}$) Using Time-Dependent Configuration Interaction with an Absorbing Potential. *J. Phys. Chem. A* **2017**, *121*, 5940–5946.

(38) Peterson, K. A.; Shepler, B. C.; Figgen, D.; Stoll, H. On the Spectroscopic and Thermochemical Properties of ClO , BrO , IO , and Their Anions. *J. Phys. Chem. A* **2006**, *110*, 13877–13883.

(39) Strobel, A.; Fischer, I.; Lochschmidt, A.; Mueller-Dethlefs, K.; Bondybey, V. E. Photodissociation Dynamics of CH_3I and CD_3I Probed by Zero Kinetic Energy Photoelectron Spectroscopy. *J. Phys. Chem.* **1994**, *98*, 2024–2032.

(40) Walter, K.; Weinkauff, R.; Boesl, U.; Schlag, E. W. Molecular Ion Spectroscopy: Mass Selected, Resonant Two-Photon Dissociation Spectra of CH_3I^+ and CD_3I^+ . *J. Chem. Phys.* **1988**, *89*, 1914–1922.

(41) Locht, R.; Dehareng, D.; Hottmann, K.; Jochims, H. W.; Baumgärtel, H.; Leyh, B. The Photoionization Dynamics of Methyl Iodide (CH_3I): A Joint Photoelectron and Mass Spectrometric Investigation. *J. Phys. B: At., Mol. Opt. Phys.* **2010**, *43*, 105101.

(42) Dietrich, P.; Burnett, N. H.; Ivanov, M.; Corkum, P. B. High-Harmonic Generation and Correlated Two-Electron Multiphoton Ionization with Elliptically Polarized Light. *Phys. Rev. A: At., Mol., Opt. Phys.* **1994**, *50*, R3585–R3588.

(43) Liao, Q.; Winney, A. H.; Lee, S. K.; Lin, Y. F.; Adhikari, P.; Li, W. Coulomb-Repulsion-Assisted Double Ionization from Doubly Excited States of Argon. *Phys. Rev. A: At., Mol., Opt. Phys.* **2017**, *96*, 023401.

(44) Torlina, L.; Ivanov, M.; Walters, Z. B.; Smirnova, O. Time-Dependent Analytical R-Matrix Approach for Strong-Field Dynamics. II. Many-Electron Systems. *Phys. Rev. A: At., Mol., Opt. Phys.* **2012**, *86*, 043409.